Journal of Science and Technology – Engineering and Technology for Sustainable Development
Volume 36, Issue 4, Month 2026, 001–009

Optimization of Energy-Absorbing Characteristics for Bio-inspired Thin-walled Structures Using an Improved Particle Swarm Optimization Method

***Nguyen Duc Hai*[1,*], *Nguyen Danh Phuong*[1], *Hoang Anh Thu*[2]**
[1]*Faculty of Mechanical and Automotive Engineering, Thanh Dong University, Hai Phong, Viet nam*
[2]*Faculty of Electrical and Electronic Engineering Technology, Dai Nam University, Ha Noi, Viet nam*
**Corresponding author email: nguyenduchai@hnu.edu.cn*

Abstract

The study focuses on optimizing the energy-absorbing characteristics of bio-inspired thin-walled structures (BTS) based on naturally inspired structural features. Three design parameters are investigated: wall thickness t, inner diameter d, and number of diaphragms n. A combined approach was employed: first, the Taguchi method with nine experiments was conducted to collect initial data; subsequently, an improved Particle Swarm Optimization (PSO) algorithm was applied to determine the influence of parameters on Specific Energy Absorption (SEA) while simultaneously searching for the optimal parameter set. The results show that the influences of parameters t, d, and n on SEA are 66%, 32.5%, and 1.5%, respectively. The optimization process using the improved PSO algorithm ultimately identified an optimal parameter set of t=1 mm, d=40.87 mm, and n=8, yielding the best SEA value of 15 kJ/kg. Validation simulations in Abaqus resulted in an SEA of 15.19 kJ/kg (1.299% deviation), which is 15.2% higher than the non-optimized configuration. The improved PSO optimization algorithm is highly effective in simplifying and solving parameter optimization problems for new energy-absorbing structures. Notably, wall thickness t is the most dominant factor, and increasing t from 1 mm to 2 mm reduces SEA by 61.5% while increasing peak force by 78.2%. Compared with a conventional circular tube of equal mass, the optimized Horsetail-Inspired Circular Tube (HICT) improves SEA by 55%, confirming its potential for lightweight automotive applications.

Keywords. Bio-inspired, particle swarm optimization, specific energy absorption, thin-walled structure, Taguchi method.

1. Introduction

The relentless advancement of automotive safety standards necessitates the continuous development of lightweight yet highly efficient energy-absorbing structures, a cornerstone of modern crashworthiness design [1-4]. Among these, thin-walled metal tubes have emerged as a dominant solution, valued for their predictable and controllable plastic deformation under axial compression, which facilitates systematic energy dissipation through progressive folding mechanisms [5-7]. Extensive research has been dedicated to evaluating and comparing the performance of various fundamental cross-sectional geometries, such as circular, square, and hexagonal tubes under axial compression and more complex loading scenarios, including oblique impact and bending [8, 9]. While these comparative studies provide valuable benchmarks, they often leave unexplored the potential for performance enhancement within a single, common cross-section [10, 11]. A significant research gap exists in the transformative redesign of the most prevalent circular tubes through structural modifications [10, 12]. This gap presents a compelling opportunity: rather than selecting from a catalog of basic shapes, can the inherent energy-absorption capacity of a circular tube be radically enhanced by reconfiguring its internal architecture? In this endeavor, bio-inspired design offers a powerful paradigm, leveraging naturally optimized patterns from evolution as blueprints for engineering innovation [13, 14]. Nature abounds with structures that masterfully balance lightweight properties and mechanical strength [15, 16]. A quintessential example is the horsetail plant, whose stem features a hollow cylindrical form internally divided by multiple thin walls into longitudinal cells. This sophisticated biological design achieves remarkable structural efficiency, inspiring a novel class of multi-cell thin-walled tubes that aim to surpass the performance limits of conventional hollow tubes by emulating this optimal natural configuration [17, 18].

This study does not aim to compare a wide variety of basic tube shapes; instead, it focuses intensively on optimizing and enhancing the vertical compression capacity of circular tubes [19, 20]. The primary

p-ISSN 3093-3242
e-ISSN 3093-3579
https://doi.org/10.51316/jst.193.etsd.2026.36.4.x
Received: Apr 10, 2026; Revised: Jun 24, 2026;
Accepted: Jun 29, 2026; Online: Jul 20, 2026

approach is to draw inspiration from an optimal natural structure, specifically the horsetail plant, to design a new generation of circular tubes with a more complex and efficient internal configuration [21-23]. The horsetail, with its cylindrical stem divided into multiple chambers by thin diaphragms, is an evolutionary masterpiece that enables it to withstand mechanical forces from the environment with minimal weight [13]. Based on this principle, we propose the concept of the Horsetail-Inspired Circular Tube [24]. This study will systematically analyze the influence of key horsetail-inspired design parameters on the energy absorption capacity of circular tubes under pure axial compression. The primary variables investigated include: the number of internal diaphragms (*n*), which creates various multi-cell configurations; the inner diameter of the tube (*d*), which dictates the available space for diaphragm arrangement; and the thickness of both the tube wall and the diaphragms (*t*). The objective is that, through the deliberate variation of these parameters, researchers can control the deformation mechanism and stress distribution, ultimately optimizing the Specific Energy Absorption (SEA) metric. By combining numerical simulation with systematic analysis, this study aims to elucidate the relationship between a bio-inspired multi-diaphragm structure and its energy absorption efficiency under axial compressive loading. The results are expected to provide concrete design guidelines for developing a new generation of high-performance, lightweight circular tube energy absorbers, which are not only efficient but also grounded in nature's optimization principles. This work is anticipated to contribute to the advancement of advanced passive safety systems.

Based on this principle, the study proposes a HICT. The performance of the HICT is significantly influenced by three key design parameters: *t*, *d*, and *n*. While previous studies have often focused on multi-objective optimization, primarily balancing SEA and the Maximum Impact Force (MIF), this research adopts a more straightforward, more focused approach: maximizing SEA as the sole optimization objective. SEA, which represents energy absorbed per unit mass, is a crucial metric for material utilization efficiency. To achieve this goal, a two-step procedure is implemented:

Step 1: Taguchi Method. A Taguchi experimental design matrix with 9 combinations of parameters *t, d*, and *n* is used to collect initial SEA data via Abaqus simulations. This allows for a qualitative assessment of the influence of each parameter.

Step 2: Influence Analysis and Optimization via an Improved Particle Swarm Optimization (PSO) Algorithm. Using the input data from the Taguchi experiments, an improved PSO algorithm is deployed to search the continuous design space for the optimal set of parameters (*t, d, n*) that maximizes SEA.

This combined approach is computationally cost-effective compared to large-scale random numerical simulations, while also leveraging the powerful global search capability of the PSO algorithm to identify the optimal configuration for the HICT efficiently.

2. Methodology

This study employs a numerical simulation approach to comprehensively analyze the energy absorption capacity of Horsetail-Inspired Circular Tubes (HICTs) under axial compressive loading. The entire procedure was conducted within the ABAQUS/Explicit software environment to ensure the consistency and reliability of the simulation results.

2.1. Geometric Design and Parameters

The research specimen is designed based on a fundamental circular tube with an outer diameter of 100 mm and a length of 350 mm, standard parameters commonly used in energy-absorbing structure studies. The distinctive feature of this research lies in modifying the internal structure of the circular tube by adding diaphragms to form multiple cells, mimicking the multi-cell configuration of a horsetail plant stem [7].

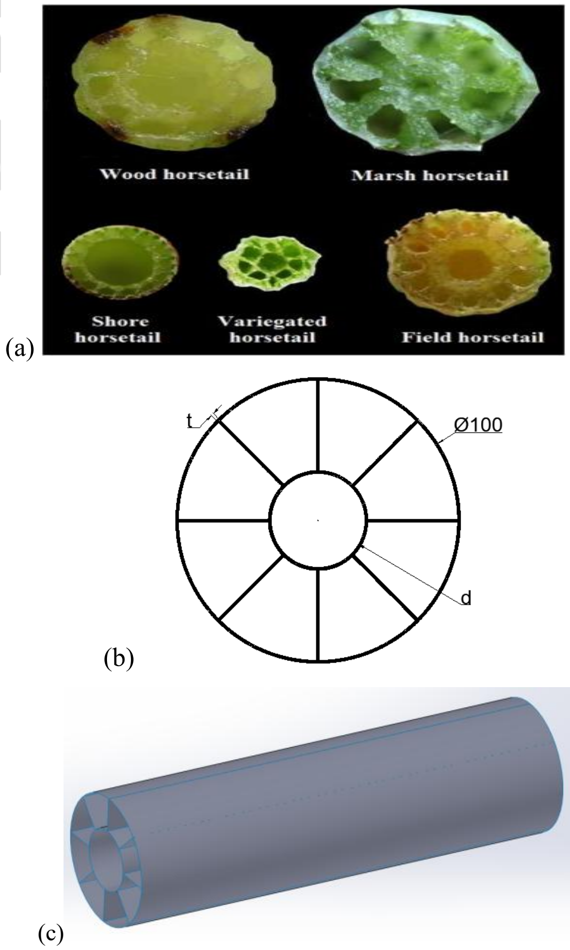

Fig. 1. Cross sections of five horsetail species

Three independent design variables were studied:

- *t* (mm): Structural thickness, encompassing both the outer wall and internal diaphragms; Investigated range: {1.0, 2.0, 3.0} mm;

- *d* (mm): Effective inner diameter; Investigated range: {20, 40, 60} mm;

- *n*: Number of diaphragms; Investigated range: {6, 8, 10}.

The material used in this study is A36 steel, with a density of 7850 kg/m³ for mass and energy calculations [25].

All simulations were performed in Abaqus/Explicit. The HICT was modeled using S4R shell elements. A mesh convergence study was conducted with element sizes of 4.0, 3.0, 2.0, 1.5, and 1.0 mm. The difference in SEA between the 2.0 mm mesh and the 1.0 mm mesh was less than 1%. Therefore, a global element size of 2.0 mm was adopted for the entire model.

With this mesh size, the finite element model of the HICT consists of 4190 number of elements of type S4R and 4,289 nodes.

The bottom plate was fully fixed, while the top plate moved downward at a constant velocity of 5 mm/min. A friction coefficient of 0.25 was used for all contacts between the plates and the tube, as well as for self-contact of the tube during deformation. A36 steel was modeled using an elastic-plastic material with Young's modulus *E* equal 200 GPa, Poisson's ratio *v* equal 0.3, and yield strength σ_y equal 250 MPa. No material failure was considered because the tube undergoes stable progressive folding without fracture. Kinetic energy was monitored and kept below 5% of internal energy throughout the simulation, ensuring quasi-static conditions.

This study is based solely on numerical simulations without direct physical experiments. However, the reliability of the finite element model is ensured through: (i) a mesh convergence study to determine the optimal element size (2.0 mm), (ii) the use of S4R shell elements suitable for large deformation and contact problems, (iii) energy monitoring (kinetic energy below 5% of internal energy) to confirm quasi-static conditions, and (iv) cross-validation between the surrogate model prediction (15.0 kJ/kg) and the Finite Element (FE) result at the optimum (15.19 kJ/kg), which shows a deviation of only 1.299%. These steps guarantee that the simulation results are sufficiently reliable within the scope of this numerical study. Future work should include experimental validation.

2.2. Taguchi Method

To obtain the input data for the improved PSO algorithm, the Taguchi method was employed to design an efficient experimental matrix. With three parameters, each at three levels, an L9 orthogonal array was selected, generating nine unique experimental combinations [26-28]. These nine HICT configurations were numerically simulated using ABAQUS software to obtain their corresponding SEA values. The results are summarized in Table 1.

Table 1. The Taguchi L9 Orthogonal Array

No.	**Case**	**Thickness t (mm)**	**Diameter d (mm)**	**Number of Diaphragms (n)**	**SEA (kJ/kg)**	**Mass (kg)**
1	TH1	1	20	6	**13.18**	**1.69**
2	TH2	1	40	8	**15.05**	**1.87**
3	TH3	1	60	10	**14.26**	**1.93**
4	TH4	2	20	8	**5.80**	**3.83**
5	TH5	2	40	10	**5.28**	**4.06**
6	TH6	2	60	6	**6.72**	**3.42**
7	TH7	3	20	10	**2.44**	**6.4**
8	TH8	3	40	6	**3.63**	**5.11**
9	TH9	3	60	8	**3.18**	**5.46**

The Taguchi L9 orthogonal array requires only nine experiments instead of 27. As shown in Table 1, 9 HICT configurations were simulated, and the obtained SEA values ranged from 2.44 kJ/kg (TH7) to 15.05 kJ/kg (TH2). These results clearly show the dominant influence of wall thickness *t* and identify the region of highest SEA at *t* equal 1 mm, *d* equal 40 mm, and *n* equal 8. The improved PSO algorithm then used these nine data points to construct a quadratic surrogate model. The final optimal design (*t*=1.0 mm, *d*=40.87 mm, *n*=8) was re-evaluated by full FE simulation, yielding an SEA of 15.19 kJ/kg, which deviates by only 1.299% from the PSO-predicted value of 15.0 kJ/kg. This very small deviation confirms that nine Taguchi samples are sufficient to reliably guide the optimization process.

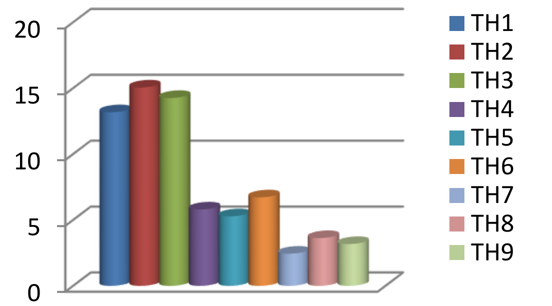

Fig. 2. Comparison of SEA values from the nine Taguchi experimental configurations

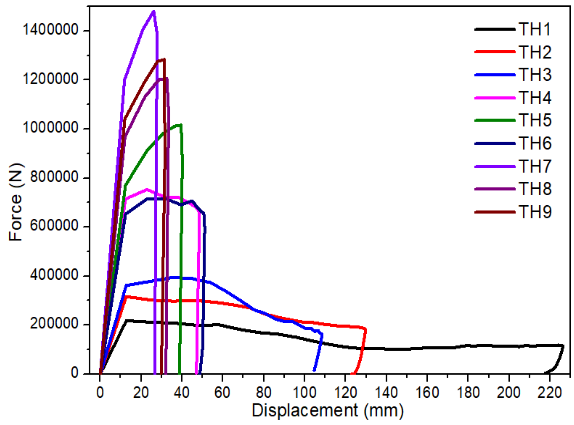

Fig. 3. Force-displacement curves of HICT configurations

Based on the results obtained in Table 1, the following preliminary assessments can be made.

Firstly, the influence of *t* is the most pronounced. As *t* increases from 1 mm to 2 mm and then to 3 mm, SEA decreases significantly from approximately 13-15 kJ/kg to 5-7 kJ/kg and then to 2-4 kJ/kg. This indicates that for the additional material mass resulting from the increase in *t*, the energy absorption capacity does not increase proportionally, thereby reducing the energy absorption efficiency per unit mass.

Secondly, the influences of *d* and *n* are more complex and interact with *t*. However, the simulation data show that the combination *t* equal 1 mm, *d* equal 40 mm, *n* equal 8 yields the highest SEA.

2.3. Improved Particle Swarm Optimization Algorithm

Unlike standard PSO which uses a constant inertia weight, this study proposes an improved PSO algorithm with an adaptive strategy and chaotic local search [29-31]. First, a quadratic surrogate model is constructed from the nine Taguchi data points (Table 1). Then, the improved PSO algorithm is deployed to search for the optimal set of parameters *t*, *d*, *n* that maximizes SEA. The optimization problem aims to maximize the objective function, the objective function is defined as:

$$Maximize\ SEA = f(t, d, n)$$

Subject to the constraints:

$$t \in \{1.0, 2.0, 3.0\} \text{ mm};$$

$$20 \le d \le 60 \text{ mm};$$

$$n \in \{6, 8, 10\}.$$

A population of 30 particles is initialized, each representing a parameter set. At each iteration, particle positions are updated based on the SEA fitness value obtained from the surrogate model, progressively converging toward the region of highest SEA. The flowchart of the algorithm is shown in Fig. 4. After the PSO proposes an optimal parameter set, a detailed finite element simulation is performed for validation.

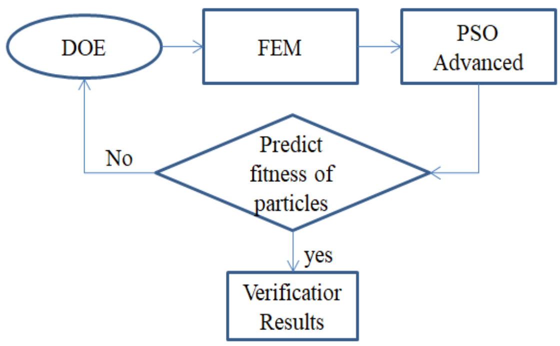

Fig 4. Flowchart of the improved PSO algorithm

3. Results and Discussion

3.1. Parameter Influence Assessment

The plots derived from the nine Taguchi experiments (shown in Fig. 5a to Fig. 5g) clearly illustrate the influence trends. Wall thickness *t* is the most influential factor. SEA reaches its maximum at *t* equal 1 mm and decreases sharply as thickness increases. The inner diameter *d* and number of diaphragms *n* exhibit non-monotonic and interdependent influences. However, *n* should be sufficient to stabilize the folding mechanism but not excessive to avoid unnecessary complexity.

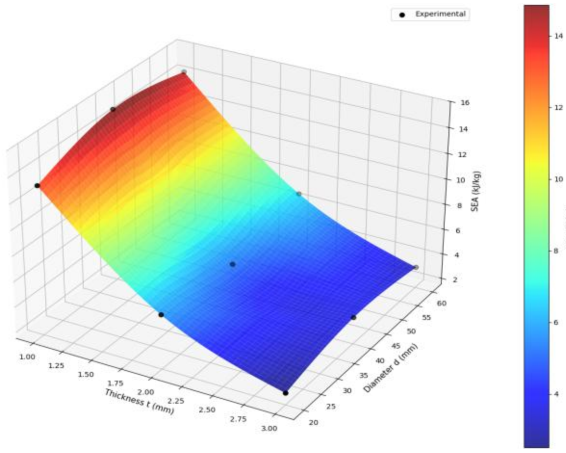

(a) Effect of *t, d* on SEA

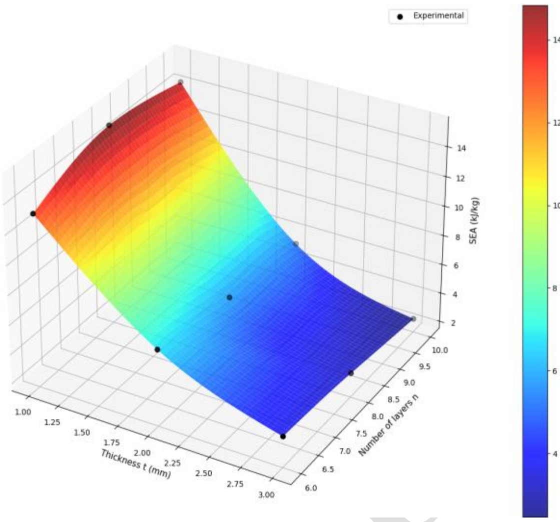

(b) Effect of *t, n* on SEA

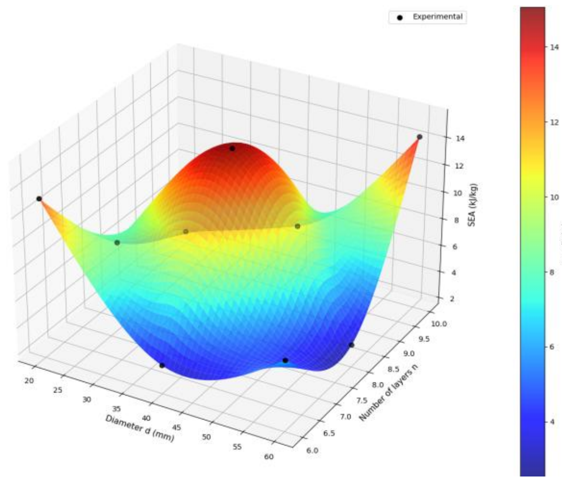

(c) Effect of *d, n* on SEA

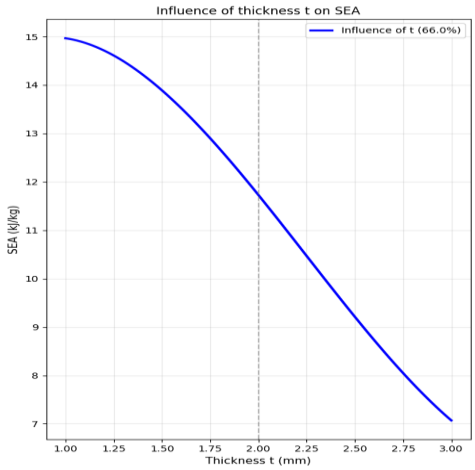

(d) Effect of *t* on SEA

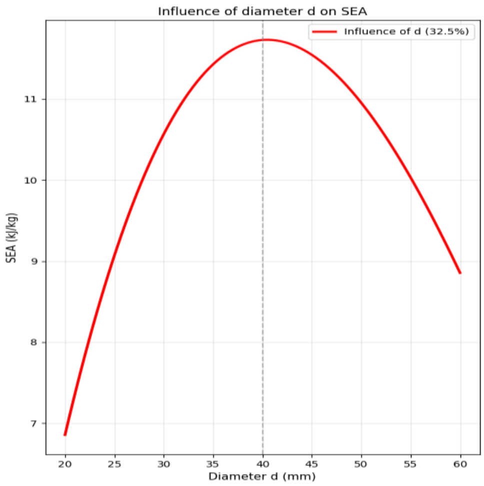

(e) Effect of *d* on SEA

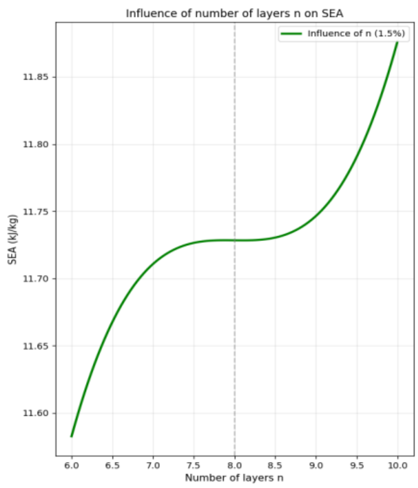

(g) Effect of *n* on SEA

Fig 5. Effect of design parameters on SEA: (a) *t-d* interaction, (b) *t-n* interaction, (c) *d-n* interaction, (d) main effect of *t*, (e) main effect of *d*, (f) main effect of *n*

The graphs displaying the obtained results demonstrate that the Taguchi method helps reduce the number of required design samples while still ensuring a sufficient number for the improved PSO optimization. The results indicate that wall thickness *t* is the dominant factor, contributing 66% to the variation in SEA, as it directly governs the cross-sectional moment of inertia and structural stiffness. The inner diameter *d* contributes 32.5%, reflecting the importance of material distribution and cross-sectional shape. Meanwhile, the number of diaphragms *n* shows a negligible influence of only 1.5%. This suggests that within the investigated range, increasing the number of diaphragms does not proportionally improve energy absorption efficiency under compressive loading. This may be due to the increase in mass not being accompanied by a corresponding improvement in the load-bearing mechanism. The convergence history of the improved PSO algorithm is shown in Fig. 6. The plot demonstrates strong convergence, which confirms that the algorithm effectively searches the design space and converges to the optimal SEA value after approximately iterations.

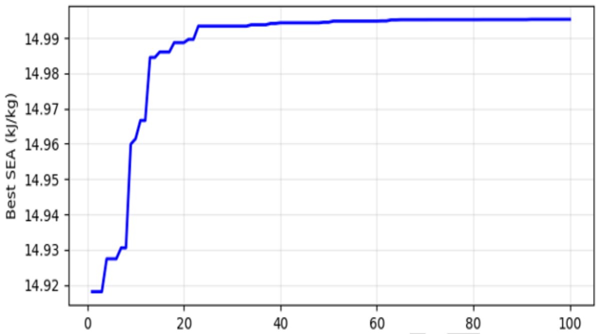

Fig. 6. Convergence history of the improved PSO algorithm

The convergence plot demonstrates strong convergence, which not only confirms that the influence of one parameter can vary significantly depending on the value of another but also indicates the existence of a shared optimal value region. Within this convergence region, the combination of (*t*) and (*d*) can achieve the highest SEA performance while also balancing other potentially conflicting objectives, such as peak force (P_{max}) or mass. This highlights the importance of simultaneously considering parameter interactions in a multi-objective optimization procedure, rather than optimizing each variable in isolation based solely on primary effect analysis.

Through the obtained plots, the complex interactive nature of the parameters and a potential optimal design space are revealed. This finding provides a crucial foundation for conducting more precise multi-objective optimization, aimed at fully exploiting the energy absorption potential of the bio-inspired structure.

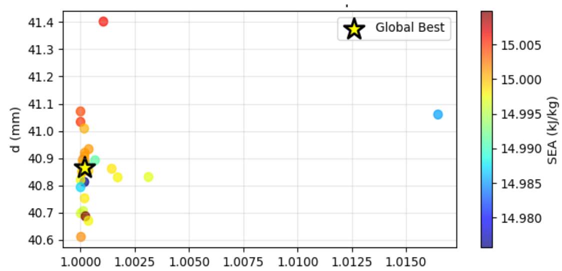

(a) Design space and the global optimum

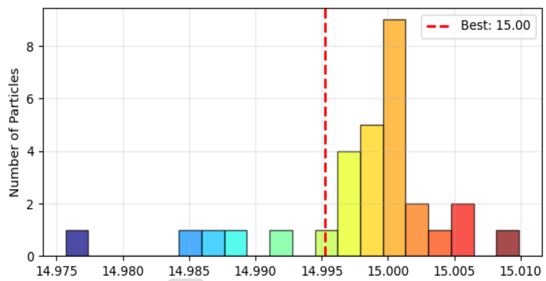

(b) Convergence history of the optimization algorithms

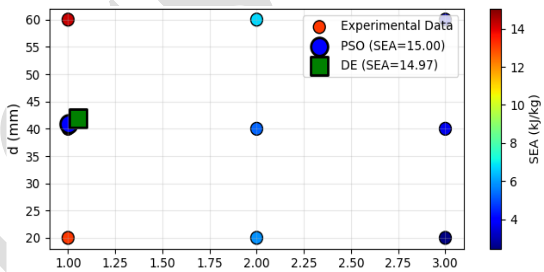

(c) Comparison of SEA values predicted by optimization algorithms

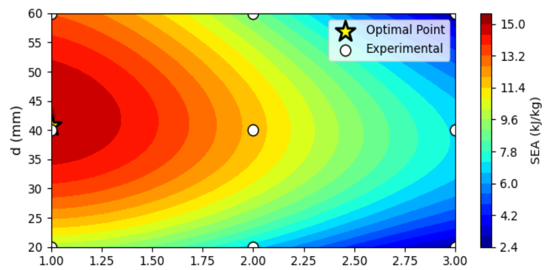

(d) Influence of wall thickness (t) on the SEA

Fig 7. Optimization results comparison: (a) design space, (b) convergence history, (c) SEA comparison, (d) influence of wall thickness *t*

3.2. Optimal Results and Model Validation

The improved PSO algorithm, after running with appropriate parameters, converged to an optimal solution. The proposed optimal parameters are: *t* equal 1.0 mm, *d* equal 40.87 mm, and *n* equal 8. A numerical simulation was performed using these optimal parameters (t = 1 mm, d = 40.87 mm, n = 8). The resulting force-displacement curve (Fig. 2) exhibits a typical stable folding behavior. The force-displacement curve of the optimized HICT is presented in Fig. 8.

To evaluate the effectiveness of the optimized HICT, it was compared with other HICT configurations having the same wall thickness *t* equal 1 mm but different parameter sets from Table 1. Configuration TH1 (*t*= 1 mm, *d* = 20 mm, *n* = 6) achieved an SEA of 13.18 kJ/kg. Configuration TH3 (*t* = 1 mm, *d* = 60 mm, *n* = 10) achieved an SEA of 14.26 kJ/kg. Configuration TH2 (*t* = 1 mm, *d* = 40 mm, *n* = 8) achieved an SEA of 15.05 kJ/kg. The optimized HICT achieved an SEA of 15.19 kJ/kg, which is 15.2% higher than TH1, 6.5% higher than TH3, and 0.93% higher than TH2. Although the improvement over TH2 is modest, it demonstrates the ability of the improved PSO to precisely converge to the continuous optimum of the inner diameter *d* equal 40.87 mm, confirming that the parameter set *t* equal 1 mm, *d* equal 40.87 mm, *n* equal 8 is indeed the best within the design space investigated.

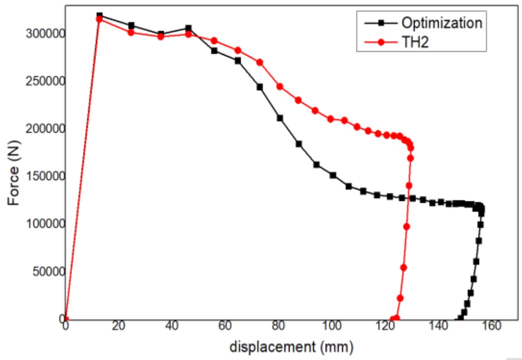

Fig. 8. Force-displacement curve of the optimal HICT configuration

The SEA value of the optimal configuration was confirmed via FEM calculation to be 15.198 kJ/kg. This value is slightly higher than the SEA value obtained from the improved PSO algorithm (15 kJ/kg). The deformation sequence of the optimized HICT at different crushing displacements is illustrated in Fig. 9. The folds initiate at the loaded end and propagate progressively downward, with no global buckling or asymmetric collapse observed, confirming the stability of the optimized design.

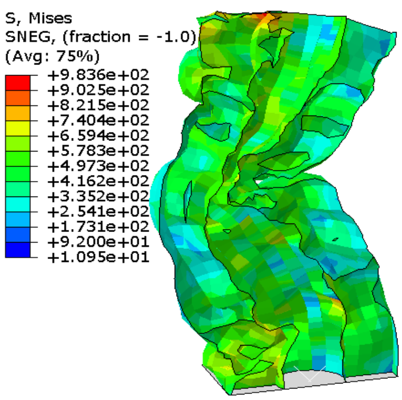

Fig 9. Crushing behavior of the optimal HICT at different displacement levels

4. Conclusion

This study presented an efficient procedure for optimizing the SEA of a bio-inspired thin-walled structure by combining the Taguchi experimental method and an improved PSO algorithm. The main conclusions drawn are as follows.

- *t* is the most decisive factor influencing SEA, with SEA decreasing sharply as *t* increases. *d* and *n* exhibit a more complex, interactive influence.

- The combined Taguchi-PSO approach provides a rapid, systematic, and cost-effective assessment of parameter influence. Based on this information, PSO can be effectively guided and deployed to precisely search for the optimal parameter set within the design space.

- The improved PSO algorithm successfully identified the optimal parameters: *t* equal 1 mm, *d* equal 40.87 mm, and *n* equal 8. This configuration yielded an SEA of 15.0 kJ/kg, which is close to the value of 15.198 kJ/kg confirmed by the validating FEA simulation, demonstrating the accurate predictive capability of the PSO.

- The results emphasize the importance of maintaining wall thickness at a suitably minimal level (to optimize SEA) while adjusting the inner diameter and number of cells to achieve a stable and efficient folding mechanism. This optimized HICT structure shows promise as a lightweight and efficient energy-absorbing component.

In future studies, we will validate the results through physical experiments, extend the optimization to more complex loading conditions, such as oblique impact, and integrate additional constraints, like Maximum Impact Force (MIF), into the optimization problem.

Acknowledgements

This work was supported by Thanh Dong University and authors thank for this support.

Declarations

Conflict of interest the authors have no conflict of interest to declare

References

[1] L. Yan and H. Xu, Lightweight composite materials in automotive engineering: State-of-the-art and future trends, Alexandria Engineering Journal, vol. 118, pp. 1–10, Apr. 2025. https://doi.org/10.1016/j.aej.2024.12.002

[2] A. D. Furlan, T. Kajaks, M. Tiong, M. Lavallière, J. L. Campos, J. Babineau, S. Haghzare, T. Ma and B. Vrkljan, Advanced vehicle technologies and road safety: A scoping review of the evidence, Accident Analysis and Prevention, vol. 147, Nov. 2020, Art. no. 105741. https://doi.org/10.1016/j.aap.2020.105741

[3] A. P. Kumar, M. D. B. Kumar, P. S. R. Sreekanth, S. K. Sahu, Q. Ma, M. M. Hanon, M. Aman, Experimental investigation on the transverse crushing performance of 3D printed polymer composite filled aluminium tubes, Journal of the Mechanical Behavior of Materials, vol. 34, iss. 1, Dec. 2025. https://doi.org/10.1515/jmbm-2025-0091

[4] Q. Ma, N. H. M. Yusof, S. K. Sahu, Y. Song, N. A. M. Radzuan, B. Sun, A. Y. Nasution, A. P. Kumar, and M. R. M. Rejab, Bio-inspired thin-walled straight and tapered tubes with variable designs subjected to multiple impact angles for building constructions, Buildings, vol. 15, iss. 4, Feb. 2025, Art. no. 620. https://doi.org/10.3390/buildings15040620

[5] Y. Chen, X. Dai, P. Fu, G. Luo, and P. Shi, A review of China's automotive industry policy: Recent developments and future trends, Journal of Traffic and Transportation Engineering (English Edition), vol. 11, iss. 5, pp. 867–895, Dec. 2024. https://doi.org/10.1016/j.jtte.2024.09.001

[6] Z. Zhang, C. Feng, L. Zhao, N. Hu, S. Hou, and X. Han, Crashworthiness analysis and optimization design of special-shaped thin-walled tubes by experiments and numerical simulation, Thin-Walled Structures, vol. 205, Dec. 2024, Art. no. 112240. https://doi.org/10.1016/j.tws.2024.112240

[7] L. Teng, D. Qingtian and L. Xinbo, Energy absorption and deformation modes of several thin-walled tubes under dynamic compression, Structures, vol. 54, pp. 890–897, Aug. 2023. https://doi.org/10.1016/j.istruc.2023.05.099

[8] X. You, Z. Xing, S. Jiang, Y. Zhu, Y. Lin, H. Qiu, R. Ni, J. Yang, D. Hui, W. Chen, Y. Chen, A review of research on aluminum alloy materials in structural engineering, Developments in the Built Environment, vol. 17, Mar. 2024, Art. no. 100319. https://doi.org/10.1016/j.dibe.2023.100319

[9] Z. Li, T. X. Yu, Z. Meng, L. Wan, Q. Zeng, and D. Ruan, Design of high-performing circular tubes of complex cross-sections guided by a single non-dimensional governing parameter, Engineering Structures, vol. 333, Apr. 2025, Art. no. 120142. https://doi.org/10.1016/j.engstruct.2025.120142

[10] J. Heath, M. Moran, and A. Dowrick, Examining qualitative cross-country comparative analysis in health: Reflective insights and methodological considerations, SSM - Qualitative Research in Health, vol. 5, Jun. 2024, Art. no. 100416. https://doi.org/10.1016/j.ssmqr.2024.100416

[11] P. Pottier, D. W. A. Noble, F. Seebacher, L. E. Schwanz, S. M. Drobniak, and S. Nakagawa, New horizons for comparative studies and meta-analyses, Trends in Ecology and Evolution, vol. 39, Mar. 2024, vol. 39, pp. 435–445. https://doi.org/10.1016/j.tree.2024.01.004

[12] E. Sánchez-García, J. Martínez-Falcó, B. Marco-Lajara, and E. Manresa-Marhuenda, Revolutionizing the circular economy through new technologies: A new era of sustainable progress, Environmental Technology and Innovation, vol. 33, Feb. 2024, Art. no. 103509. https://doi.org/10.1016/j.eti.2023.103509

[13] Y. Wang, I.-K. Cai, Z. Wang, X. Li, S. Wang and J. Pan, Bio-inspired circular tubes with enhanced lateral energy absorption, Composite Structures, vol. 378, Feb. 2026, Art. no. 119954. https://doi.org/10.1016/j.compstruct.2025.119954

[14] A. Y. Nasution, M. R. M. Rejab, J. P. Siregar, and Q. Ma, Effect of number of triggers and shape of crash box on energy absorption during experimental collision, ARPN Journal of Engineering and Applied Sciences, 2024, vol. 19, pp. 1–10.

[15] N. V. Hinh, T. H. Phong and N. D. Hai, A Novel evaluate the ultimate strength of plate having cutout under in-plane compression, International Journal of Mechanical Engineering and Applications, vol. 12, iss. 2, pp. 50–58, 2024. https://doi.org/10.11648/j.ijmea.20241202.12

[16] Y. Tian, P. Zhou, F. A. Hassan, O. Al-Khatib, F. Alshammari and N. Mazraoui, Crashworthiness and technoeconomic assessment of bioinspired GFRP PP tubes using experiments, numerical modeling and artificial neural networks, Scientific Reports, vol. 16, Mar. 2026, Art. no. 15592. https://doi.org/10.1038/s41598-026-40978-6

[17] G. Murali, A. Thakur, S. Dixit, S. Singh, and A. Stefańska, Biomimicry in construction: Innovations in energy absorption through bio-inspired structural designs, Sustainable Materials and Technologies, vol. 45, Oct. 2025, Art. no. e01628. https://doi.org/10.1016/j.susmat.2025.e01628

[18] C. Husby, Biology and functional ecology of *Equisetum* with emphasis on the giant horsetails, The Botanical Review, vol. 79, pp. 147–177, Jun. 2013. https://doi.org/10.1007/s12229-013-9104-9

[19] Y. Liu, J. Cai, and J. Feng, Buckling suppression of a thin-walled Miura-origami patterned tube, PLOS One, vol. 17, Jul. 2022, Art. no. e0262928. https://doi.org/10.1371/journal.pone.0262928

[20] Z. Cheng, J. Du, S. Jia, C. Xiao, F. Jiao and Y. Hong, Impact of tube shapes on the energy storage and thermal-hydraulic performances of finned latent heat energy storage systems, Case Studies in Thermal Engineering, vol. 67, Mar. 2025, Art. no. 105827. https://doi.org/10.1016/j.csite.2025.105827

[21] X. He, Z. Li, J. Wang, and H. Yu, Effects of tube cross-sectional shapes on flow pattern, liquid film and heat transfer of *n*-pentane across tube bundles, Chinese Journal of Chemical Engineering, vol. 60, pp. 16–25, Aug. 2023. https://doi.org/10.1016/j.cjche.2023.01.003

[22] N. S. Ha and G. Lu, A review of recent research on bio-inspired structures and materials for energy absorption applications, Composites Part B: Engineering, vol. 181, Jan. 2020, Art. no. 107496. https://doi.org/10.1016/j.compositesb.2019.107496

[23] A. Sandak and K. Butina Ogorelec, Bioinspired building materials-lessons from nature, Frontiers in Materials, vol. 10, Mar. 2023, Art. no. 1164529. https://doi.org/10.3389/fmats.2023.1164529

[24] M. A. A. El-Baky, S. A. Abdalaziz, M. A. Hassan and M. M. A. Allah, Integrating bio-inspired concepts into lightweight sustainable crashworthy designs under lateral loading scenario, Fibers and Polymers, vol. 26, Jun. 2025, pp. 3585–3600. https://doi.org/10.1007/s12221-025-01938-4

[25] Z. Ahmad and D. P. Thambiratnam, Dynamic computer simulation and energy absorption of foam-filled conical tubes under axial impact loading, Computers and Structures, vol. 87, pp. 186–197, Feb. 2009. https://doi.org/10.1016/j.compstruc.2008.10.004

[26] N. Li, C. Shi, Z. Zhang, H. Wang and Y. Liu, A review on mixture design methods for geopolymer concrete, Composites Part B: Engineering, vol. 178, Dec. 2019, Art. no. 107490. https://doi.org/10.1016/j.compositesb.2019.107490

[27] S. Sahoo, R. K. Dalei, S. K. Rath, and U. K. Sahu, Selection of PSO parameters based on Taguchi design-ANOVA-ANN methodology for missile gliding trajectory optimization, Cognitive Robotics, vol. 3, pp. 158–172, Dec. 2023. https://doi.org/10.1016/j.cogr.2023.10.002

[28] M. W. Hisam, A. A. Dar, M. O. Elrasheed, M. S. Khan, R. Gera and I. Azad, The Versatility of the Taguchi Method: Optimizing experiments across diverse disciplines, Journal of Statistical Theory and Applications, vol. 23, pp. 365–389, May 2024. https://doi.org/10.2991/jsta.d.240411.001

[29] Y. O. M. Sekyere, F. B. Effah and P. Y. Okyere, An enhanced particle swarm optimization algorithm via adaptive dynamic inertia weight and acceleration coefficients, Journal of Electronics and Electrical Engineering, Jan. 2024. https://doi.org/10.37256/jeee.3120243868

[30] A. Nickabadi, M. M. Ebadzadeh, and R. Safabakhsh, A novel particle swarm optimization algorithm with adaptive inertia weight, Applied Soft Computing, vol. 11, iss. 4, pp. 3658–3670, Jun. 2011. https://doi.org/10.1016/j.asoc.2011.01.037

[31] H. Xu, Q. Deng, Z. Zhang and S. Lin, A hybrid differential evolution particle swarm optimization algorithm based on dynamic strategies, Scientific Reports, vol. 15, Feb. 2025, Art. no. 4518. https://doi.org/10.1038/s41598-025-86441-5